Batteries & Supercaps

Research Article
doi.org/10.1002/batt.202300226

Chemistry Europe
European Chemical Societies Publishing

www.batteries-supercaps.org

Special Collection

On the Viability of Lithium Bis(fluorosulfonyl)imide as Electrolyte Salt for Use in Lithium-Ion Capacitors

Philipp Schweigart,*[a] Obinna Egwu Eleri,[c] Inger-Emma Nylund,[a] Samson Yuxiu Lai,[b] Fengliu Lou,[d] and Ann Mari Svensson*[a]

Lithium-ion capacitors (LICs) represent promising high-power energy storage devices, most commonly composed of a lithium-ion intercalation anode (e.g., graphite or hard carbon), a supercapacitor activated carbon (AC) cathode, and an electrolyte with 1 M $LiPF_6$ in carbonate solvents. $LiPF_6$ is susceptible to hydrolysis, forming HF, which leads to challenges for disassembly and recycling, risks during hazardous events, and extensive energy consumption during production. Here, we report on the feasibility of replacing $LiPF_6$ with the non-hydrolysing salt LiFSI for use with AC electrodes. Based on voltage hold measurements in a half-cell setup, good long-term stability is achieved with an upper cut-off voltage of 3.95 V vs. Li/Li^+, potentially enabling cell voltages of ~3.8 V when combined with graphite or silicon-based anodes (operating at ~0.1 V vs. Li/Li^+) in LIC full cells. The lower cut-off voltage was determined to be 2.15 V vs. Li/Li^+. The systematic comparison of CV, leakage current analysis and capacity retention upon voltage hold highlights the importance of the latter method to provide a realistic assessment of the electrochemical stability window (ESW) of LiFSI on a commercial AC electrode. The morphological and surface-chemical post-mortem analysis of AC electrodes used with LiFSI revealed that the oxidation of the FSI anion, as evidenced by the presence of new S 2p and N 1s features in the XPS spectra, and an increasing number of oxygenated species on the AC were the main processes causing capacity fade at positive polarization.

Introduction

The rising demand for renewable energy has prompted the exploration and research of novel electrochemical energy storage devices. Bridging the gap between high power densities of supercapacitors (SCs) and high energy densities of lithium-ion batteries (LIBs), lithium-ion capacitors (LICs) represent a promising solution for fast-rate harvesting, storage and delivery of electrical energy.[1,2] The most common and technologically viable[2] configuration of a LIC consists of a LIB-type anode (e.g., graphite or hard carbon) based on the faradaic insertion/deinsertion of Li-ions combined with high surface area activated carbon (AC) as the SC-type cathode based on the reversible electrostatic adsorption/desorption of ions from an organic, Li-salt containing electrolyte. The salt lithium hexafluorophosphate ($LiPF_6$) dissolved in carbonate solvents such as ethylene carbonate (EC), dimethyl carbonate (DMC) or diethyl carbonate (DEC) is considered as standard electrolyte in LICs[3,4] owing to its established anode chemistry, favorable capacitances of about 100 F/g when coupled with AC electrodes[5,6] and high ionic conductivity[7] ensuring suitability for high-power applications.

A key metric for LICs is the electrochemical interaction of the electrolyte with the AC cathode as a function of potential. Upon charge/discharge of the LIC, anion adsorption/desorption occurs as the AC potential varies between the open circuit potential (OCP, ~3 V vs. Li/Li^+) and a positive vertex potential (typically 4.0–4.4 V vs. Li/Li^+). The use of a pre-lithiated anode enables the AC cathode to exploit the potential regime negative of its OCP, i.e., take advantage of the adsorption/desorption of Li^+ supplied by the pre-lithiated anode via a "rocking-chair mechanism"[1] (see Figure S1A and B in the Supporting Information for principal sketches of the voltage profiles of LICs with and without a pre-lithiated anode). While the extended potential swing provided by a pre-lithiated anode endows higher cell capacity, it is a key requirement that the electrochemical stability window (ESW) of the electrolyte on the AC cathode is also wide enough. The oxidative or reductive electrolyte decomposition upon positive or negative overcharging, respectively, is facilitated by the confinement of electrolyte

[a] P. Schweigart, Dr. I.-E. Nylund, Prof. A. M. Svensson
Department of Materials Science and Engineering
Norwegian University of Science and Technology
Trondheim (Norway)
E-mail: philipp.schweigart@ntnu.no
annmari.svensson@ntnu.no

[b] Dr. S. Y. Lai
Battery Technology Department
Institute for Energy Technology
Kjeller (Norway)

[c] O. E. Eleri
Department of Energy and Petroleum Engineering
University of Stavanger
Stavanger (Norway)

[d] Dr. F. Lou
Beyonder AS
Stokkamyrveien 30, Sandnes (Norway)

Supporting information for this article is available on the WWW under https://doi.org/10.1002/batt.202300226

Special Collection An invited contribution to a Special Collection dedicated to NordBatt 2022 conference

moieties in the micropores of the AC, its high surface area (> 1000 $m^2 g^{-1}$) with catalytic properties, and the presence of reactive oxygen surface groups.[8,9] The electrolyte decomposition encompasses gassing reactions,[10] the deposition of pore-blocking reaction products,[8] and crosstalk of dissolved decomposition products with other cell components[11] eventually leading to early device failure.

While the majority of reports have investigated the aging and degradation mechanisms of state-of-the art SC electrolytes such as $TEABF_4$ in acetonitrile (AN) or propylene carbonate (PC),[12–14] much less research has been done on the interaction of AC with lithium-containing electrolytes. As for $LiPF_6$ in EC/DMC (1 : 1 v/v), an upper cutoff potential of 4.2 V vs. Li/Li^+ has been reported, however extended exposure to this potential for several hundred hours revealed the oxidative decomposition of PF_6^- anion, deposition of carbonate due to EC decomposition, and formation of surface defects on the AC as degradation pathways.[15] In another study involving LIC full cells, the generation of HF acid at the AC cathode at a potential of 4.27 V vs. Li/Li^+ was found to result from oxidative decomposition of the PF_6^- anion followed by reaction with residual water or organic solvent, leading to the deposition of LiF on the graphite anode.[11] In addition to electrochemical decomposition, $LiPF_6$ is known to react spontaneously with water, which is difficult to remove entirely from the electrolyte. Deposition of hydrolysis products and/or their initiation of parasitic side reactions are likely to adversely affect device performance.

Considering the aforementioned limitations of $LiPF_6$ regarding its chemical and electrochemical stability, various alternative salts have been considered for use in LICs.[16] In recent years, the salt lithium bis(fluorosulfonyl)imide (LiFSI) has attracted a lot of attention due to its superior performance in combination with graphite[17] or silicon[18] anodes, on-par conductivity with $LiPF_6$ in carbonate solvents, low propensity towards hydrolysis,[19] and recent progress in large-scale synthesis[20] with the prospect of chloride-free and HF-free synthesis pathways.[21] The low propensity towards hydrolysis could significantly reduce the dry room manufacturing requirements during production of devices. Although extensively covered in numerous battery-related articles, the reports dedicated to the suitability of LiFSI for application in LICs, and specifically its behavior when confined in microporous carbon electrodes, are limited. In a recent study, a stability limit of 4.3 V vs. Li/Li^+ has been reported for AC exposed to 1 M LiFSI dissolved in PC.[22] However, no insight into the degradation mechanism upon long-term aging was provided, and the use of graphite as the LIC anode[3,4,23] necessitates the use of EC/DMC because of ion-solvent cointercalation into the host structure when using PC.[7]

A key challenge when implementing LiFSI-based salts for energy storage devices is the corrosion of the aluminum current collector at high anodic potentials.[19] The tendency of aluminum to undergo dissolution in the electrolyte is mostly ascribed to the solubility of the $Al[FSI]^-$ complex, which varies depending on the type of solvent, the salt concentration,[24] in addition to chloride contamination accelerating pitting corrosion.[19] In most works, the stability of the aluminum current collector is assessed through cyclic voltammetry (CV), which suggests effective passivation up to 4.3 V[25] and even 5 V vs. Li/Li^+[19] for LiFSI in EC/EMC. However, the use of few cycles in CV and the comparatively short time spent at the positive potentials does not comply with long-term constant voltage tests used for testing of supercapacitor materials.[26] The use of chronoamperometry (CA), which reflects the testing conditions applied in voltage hold tests, is only reported in a few publications.[19,27] For LiFSI in carbonate solvents, exposure to constant potential of 4.2 V led to stable responses at room temperature, but the exposure time of 3.5 hours was rather short compared to voltage hold tests intended to last several hundred hours[26] and no post-mortem analysis was provided.[19] More insight is needed regarding the verdicts gained from CV and CA, the stability of passivation layers at extended exposure to elevated constant potentials, and the degree to which the current collector affects the electrochemical integrity of AC electrodes.

In view of the limited understanding of the stability of LiFSI-based electrolytes for LICs, and the fact that the reported anodic cut-off potentials in carbonate electrolytes in general are close to the expected stability limit of the aluminum current collector for this salt, the present study comprehensively investigates the aging and degradation behavior of AC in the presence of 1 M LiFSI in EC/DMC (1 : 1 wt%) electrolyte. In detail, the ESW in positive and negative direction are evaluated for AC electrodes in half-cell setup by comparative use of CV and voltage hold tests, corresponding to short-term transient and long-term potentiostatic methods, respectively. Post-mortem analysis further sheds light on the mechanism behind capacity fade of AC electrodes operating within and outside their respective ESWs. The aspect of aluminum corrosion in LiFSI is revisited, in light of high-voltage AC electrodes, including the use of carbon-primed aluminum current collectors, which are commonly used in battery and supercapacitor electrodes to minimize contact resistance of active material and current collector.[15,28] Finally, the ESW and rate performance are compared to the state-of-the art $LiPF_6$ in EC/DMC (1 : 1 wt%) electrolyte on the same AC. This study puts forward a guideline to determine the stable voltage operating window of AC cathodes for LICs towards better device performance, safety and longevity.

Results and Discussion

Current collector stability in LiFSI-based electrolyte

It is crucial that the current collector material is stable when intended for use in high-voltage capacitors. Therefore, a close examination of the behavior of uncoated aluminum foil (Al) and carbon-primed aluminum foil (c-Al) in the presence of LiFSI is given in Figure 1. Figure 1(A and D) presents CVs of the respective foils cycled between 3.15 V and 4.4 V vs. Li/Li^+. A slow scan rate of 0.1 $mV s^{-1}$ is chosen to enable observation of slow redox reactions.[24] In addition, CA of Al and c-Al was performed at selected potentials (Figure 1B and E) for 24 h to emulate the conditions the current collector is subjected to in a fully charged LIC. Observation of the current profile allows the

Research Article
doi.org/10.1002/batt.202300226
Chemistry Europe
European Chemical Societies Publishing

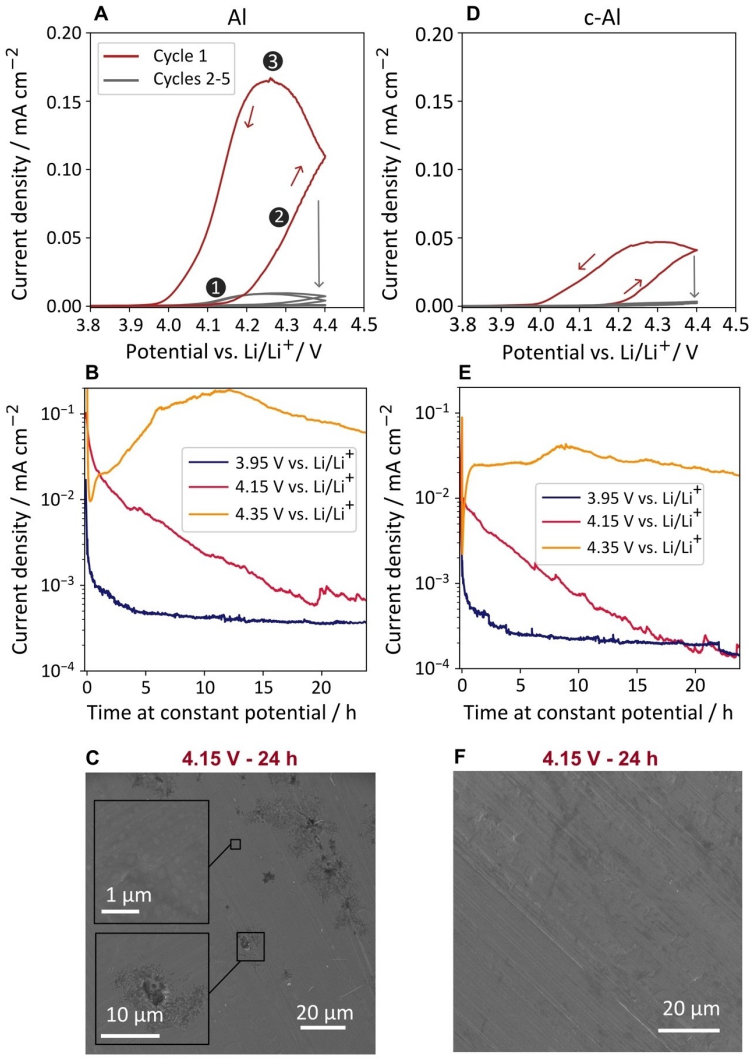

Figure 1. Cyclic voltammograms of LiFSI on A) Al electrode and D) c-Al electrode. Chronoamperograms of B) Al electrode and E) c-Al electrode in LiFSI at selected potentials. Post-mortem SEM of C) Al electrode and F) c-Al electrode with removed carbon coating after exposure to 4.15 V vs. Li/Li$^+$ for 24 h in LiFSI.

assessment of parasitic processes, with a non-declining profile indicating corrosion and/or other degradation processes.[24,29] Post-mortem electron micrographs of Al and c-Al held at 4.15 V vs. Li/Li$^+$ for 24 h are presented in Figure 1(C and F), respectively, to check for the occurrence of corrosion pits and deposits on the aluminum surface.

The first cycle in the CV obtained for the Al electrode in Figure 1(A) (red curve) possesses several regions. At point 1, the current exhibits a low increase. From point 2 at ~4.1 V vs. Li/Li$^+$, the current magnitude increases strongly. The current hysteresis at point 3, i.e., an increase in current in the back scan (see arrows) is commonly attributed to pitting corrosion and dissolution processes.[19,27,30] A Tafel plot of the CV curve is provided in the Supporting Information, Figure S6, and clearly shows two Tafel slopes, indicating that the nature of the faradaic reactions are changing at a potential of around 4.1 V. It is reasonable to assume that the currents above 4.1 V result from both the corrosive dissolution of aluminum and product formation. On the other hand, the drastically lowered current in subsequent cycles (grey curves) is commonly attributed to effective electrode passivation[27,31] which suggests a stable behavior up to a potential of 4.4 V. Therefore, the CVs do not allow an unambiguous interpretation in terms of the onset potential of aluminum dissolution.

To complement the findings from CV and emulate the conditions the current collector is subjected to in a fully charged LIC, CA experiments at selected voltages were performed (Figure 1C). The premise for interpretation of the current profile is that a declining current represents a passivation-type process, whereas a non-declining and irregular profile indicates corrosion or other parasitic processes.[24,29] Upon potential step to 3.95 V vs. Li/Li$^+$, the current rapidly declines towards very low values in the range of 10^{-3} mA cm^{-2}, possibly caused by charging of the electrical double layer without significant faradaic currents. Exposure to 4.15 V vs. Li/Li$^+$ also reveals a steadily declining current, however higher in magnitude, indicating a higher reactivity of aluminum and/or a higher rate of faradaic reactions. As revealed by the post-

mortem SEM micrographs shown in Figure 1(C), despite declining current, corrosion pits in diameters of 1 to 5 microns have been created, together with the deposition of a surface film detected throughout the electrode surface stemming from anodic decomposition of the LiFSI salt and/or the solvent. This indicates that pitting corrosion and passivation layer formation happens simultaneously upon extended exposure to 4.15 V vs. Li/Li^+. Exposure of Al to 4.35 V vs. Li/Li^+ exhibits a very irregular current profile, clearly stemming from pitting corrosion which was visually observed after retrieval of the electrode. It is noteworthy that a qualitatively similar current profile at 4.35 V vs. Li/Li^+ is obtained with the electrode first exposed to the CV protocol of Figure 1A (see Figure S7), illustrating that the presumed passivation film after repeated voltammetric sweeping is not stable enough to withstand long-term exposure at this potential.

To our knowledge, the combined use of cyclic voltammetry and chronoamperometry is rarely practiced in previous studies. Based on CV, LiFSI-based carbonate electrolytes were deemed passivating for vertex potentials as high as 4.3 V[25] or even 5 V.[19] Our results highlight that the current collector must in addition be subjected to CA protocols, which unveil its durability at longer timescales. The corrosion onset potential as determined by CA, here $\approx$4.15 V, is often substantially lower than suggested by CV.

The CV profiles of c-Al exposed to LiFSI (Figure 1D) resemble those of Al, however, with suppressed oxidation current densities compared to Figure 1(A), suggesting that the carbon priming reduces the area of the Al exposed to the electrolyte (see Figure S5 for a SEM micrograph of pristine c-Al). A Tafel plot of the first cycle CV is shown in the Supporting Information (Figure S6B), which again exhibits a change of the Tafel slope around 4.15 V pointing towards a change in reaction mechanism at this potential. Chronoamperograms in Figure 1(E) show the same trend as with Al (Figure 1B), however tending toward a lower current magnitude for c-Al at 4.15 V vs. Li/Li^+ (10^{-4} mA cm^{-2}), in line with the fact that a significant amount of Al is shielded from the electrolyte. The enhanced durability at 4.15 vs. Li/Li^+ was verified by the post-mortem micrograph of the foil showing the absence of corrosion pits (Figure 1E), with some darkened spots possibly due to the removal procedure of the carbon priming prior to imaging. However, since the pristine c-Al foil has micron-sized voids exposing free aluminum surface, it can be argued that the carbon interlayer can greatly suppress, but not entirely prevent the occurrence of aluminum dissolution, especially when the electrode is held at 4.15 V for longer timespans. While the carbon-primed current collector used in this work fulfills the dual role of contact resistance reduction and corrosion mitigation, the preparation of a void-free carbonaceous interlayer could potentially render aluminum current collectors even more stable against corrosive electrolytes, beyond 4.15 V vs. Li/Li^+.

Finally, it must be noted trace amounts of chloride (Cl^-) in the electrolyte can have a substantial influence on the corrosion tendency. Kühnel et al. recognized a completely different dissolution behavior of the ionic liquid Pyr_{14}-FSI containing 2 ppm and $<$1 ppm Cl^- residues, with the first electrolyte readily dissolving aluminum.[32] With the provided LiFSI salt (see experimental), the maximum Cl^- concentration in the EC/DMC +1 M LiFSI electrolyte corresponds to 14 ppm. Despite the significantly different dissolution behavior of aluminum exposed to FSI-based carbonate electrolytes and ionic liquids (with the latter generally being less prone to initiate corrosion), it can certainly be expected that the residual chloride content adversely impacts the maximum attainable stable potential, especially at constant potential conditions. Thus, we believe that the detected long-term stability limit of 4.15 V can certainly be increased if Cl^- residues stemming from salt, solvent and all other cell components are brought to a minimum.

Transient and long-term electrochemical stability of AC electrode in LiFSI-based electrolytes

With the established results of current collector stability, the ESW of AC electrodes in positive and negative direction is addressed. In Figure 2(A), CVs are presented in which the vertex potential is increased by 100 mV in subsequent scans while Figure 2(B) indicates the extracted S-value for each scan as a function of vertex potential. A departure of the S-value from zero is attributed to the occurrence of faradaic, non-reversible processes in the forward scan, indicative of electrolyte or electrode degradation. Figure 2(C) presents the capacity retention upon voltage hold experiments at the denoted constant voltage. In Figure 2(D), leakage currents extracted from the first 25 h of voltage hold are presented.

For small potential excursions, the CVs exhibit a box-shaped profile, characteristic for capacitive charge storage involving the adsorption of FSI^- anions during the forward scan from OCV of 3.15 V vs. Li/Li^+ to the positive vertex potential, followed by FSI^- desorption in the backward scan. As the positive vertex potential is increased, irreversible faradaic reactions stemming from decomposition reactions of the electrolyte and/or the host material cause a marked rise of the current in the voltammogram. This is well reflected by a departure of the S-value from zero, which shows a significant rise for vertex potentials higher than 3.75 V vs. Li/Li^+ (Figure 2B). The increasing extent of decomposition at higher anodic potentials agrees with long-term voltage hold tests in Figure 2(C), showing only minor degradation at a constant voltage of 3.75 V vs. Li/Li^+, a capacity retention well over the end-of-life-criterion of 80% for 3.95 V vs. Li/Li^+, followed by more pronounced capacity fade at 4.15 V vs. Li/Li^+, and serious capacity fade at 4.35 V vs. Li/Li^+. In line with the trend of capacity fading for increasing potential, leakage current profiles (Figure 2D) reveal higher current plateaus. The decaying leakage current at 4.15 V vs. Li/Li^+ is in line with CA experiment in Figure 1(E) (red curve), demonstrating that the observed capacity fade for potentials $\leq$4.15 V vs. Li/Li^+ can mainly be attributed to the decomposition of AC and/or electrolyte with negligible contribution of current collector degradation. In contrast, the irregular current profile at 4.35 V vs. Li/Li^+ identifies current collector dissolution as the main source of degradation, in line with the CA in Figure 1(B) (orange curve). Overall, the anodic limit of the system AC/LiFSI is lower

Research Article
doi.org/10.1002/batt.202300226
Chemistry Europe
European Chemical Societies Publishing

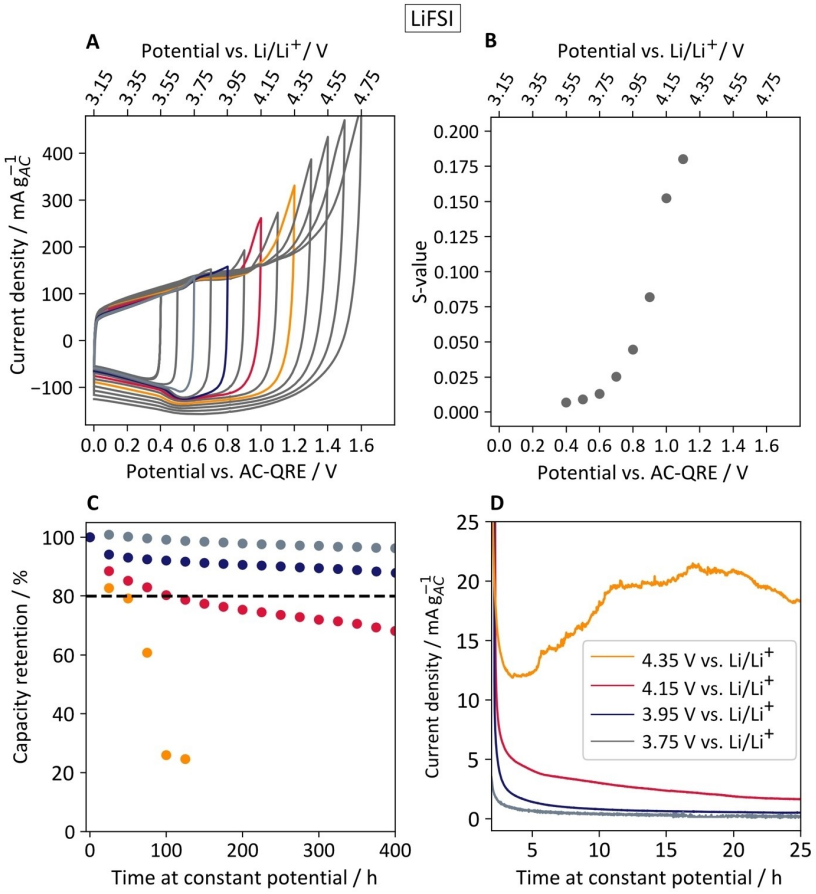

Figure 2. Anodic stability of LiFSI on AC in three-electrode half-cell setup. A) Cyclic voltammograms with gradual increase of vertex potential. B) S-values extracted from CVs. C) Capacity retention during voltage hold tests at selected potentials. D) Leakage currents during first 25 h of voltage hold.

than the corrosion onset potential of the system c-Al/LiFSI, i.e., the current collector does not significantly limit the electrochemical performance of the AC electrode up to a potential of 4.15 V vs. Li/Li$^+$.

However, it is worth remarking that an important limitation of half-cell measurements is the ability to fix the working electrode potential, which does not necessarily apply to LIC full cells. In studies on LIC full cells, a gradual shift of the AC cathode's vertex potential has been observed, eventually reaching 4.30 V vs. Li/Li$^+$ due to Li loss at the pre-lithiated anode.[3,33] This would initiate current collector dissolution in the case of a LiFSI-based electrolyte. Therefore, a realistic application of an LiFSI-based electrolyte implies that a substantial potential drift in the anodic direction must be prevented, so that the electrode resides well within the non-corrosive potential regime of the current collector stability.

In contrast to positive polarization, the correlation between long-term stability attained in voltage hold tests, voltammetric pre-tests and leakage current magnitude is less evident for negative polarization, as seen in Figure 3.

The CV profile of negatively polarized AC (Figure 3A) is a result of the reversible adsorption of Li$^+$ ions during potential sweep from OCV to moderate negative vertex potentials, followed by Li$^+$ desorption in the backward scan. As the voltage window is successively opened, the transition from purely capacitive behavior towards the predominant occurrence of parasitic side-reactions is not as evident as for positively polarized AC, with the current at the vertex point evening out at very wide window openings due to unknown reasons. Also, the S-values do not convey a clear trend concerning the limit of electrochemical stability. This can be attributed to two effects complicating the exact determination of ESW by means of CV: (1) irreversible processes in the backward scan (denoted with *) cause the S-value to take up values closer to zero, and (2) small faradaic currents are masked by the large double layer capacitance possessed by microporous capacitive materials. Thus, small and smeared out peaks in CV may be erroneously interpreted as pseudocapacitance instead of irreversible decomposition reactions, leading to overestimation of the ESW. Results from voltage hold experiments shown in Figure 3(C) indicate that there is a pronounced difference in the lifetime of electrodes exposed to 2.15 V and 1.95 V vs. Li/Li$^+$, while the CV curves with the former and latter vertex potentials (green and blue curves in Figure 3A) would not allow a clear judgment about the true ESW.

Interestingly, leakage current plateaus only reveal a small increase for more cathodic hold potentials, despite the differences in capacity retention between electrodes exposed to

Research Article
doi.org/10.1002/batt.202300226
Chemistry Europe
European Chemical Societies Publishing

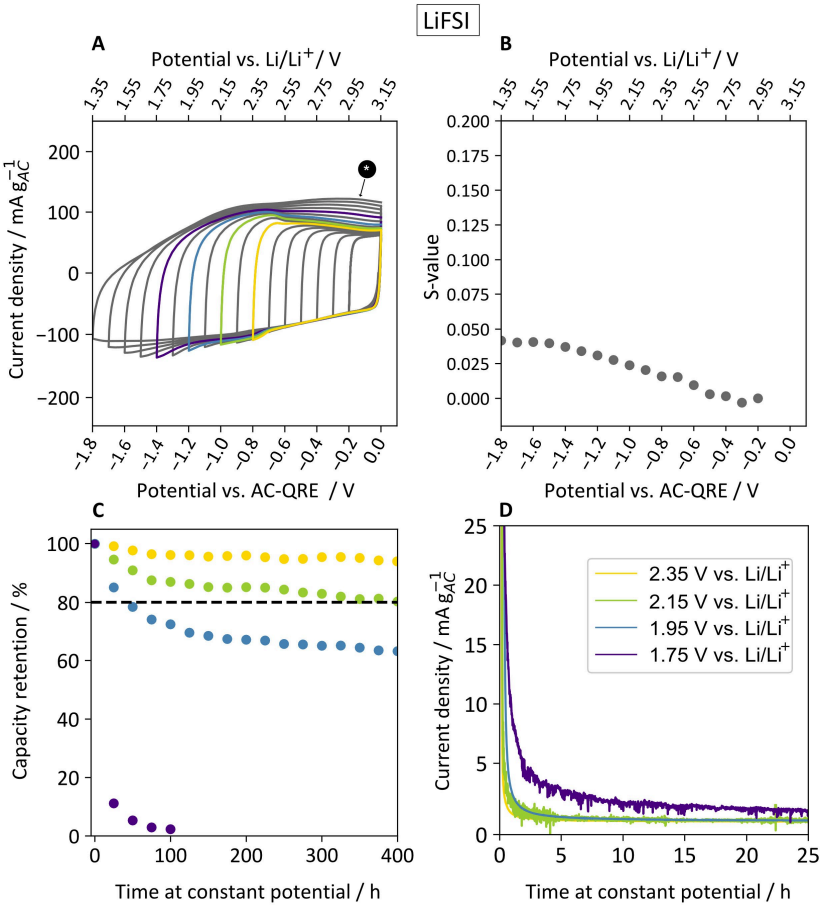

Figure 3. Cathodic stability of LiFSI on AC in three-electrode half-cell setup. A) Cyclic voltammograms with gradual lowering of vertex potential. B) S-value extracted from CVs. C) Capacity retention during voltage hold tests at selected potentials. D) Leakage currents during first 25 h of voltage hold test.

2.35 V, 2.15 V, and 1.95 V vs. Li/Li^+. This implies that slow degradation processes have in fact a strong influence on the extent of degradation over a longer timescale. The discrepancy in leakage current magnitude between positive and negative polarization (see Figures 2D and 3D) illustrates that there is no clear relation between the absolute leakage current magnitude and capacity fade, which can be attributed to a different reaction mechanism depending on electrode potential and polarity. Two hypothetical reactions, both consuming the same charge, can potentially result in different degrees of damage, e.g., by producing soluble products in one case and producing a solid product resulting in pore clogging in the other case.

In the recent study of Sun et al.,[22] an ESW of 2.3 to 3.8 V vs. Li/Li^+ was determined for AC electrodes in a similar electrolyte (1 M LiFSI in the solvent mixture of EC:PC:DEC = 3:1:4), based on CV scans and S-values. Also, the limitations of CVs for determination of ESWs were recognized, and the criterion $d^2S/dU^2 < 0.05$, was used.[34] Sun et al. also reported diverging values for the anodic stability limit for AC electrodes combined with 1 M LiFSI in PC solvent, 4.3 V based on voltage hold measurements, and 3.9 V based on S-values. It should be noted that the scan rates they used were 1 to 2 mV/s, which are higher than those used in the present study, which will typically tend to widen the measured ESW due to the slow kinetics of the electrolyte decomposition reactions.[35]

Post-mortem SEM of cycled AC electrodes in LiFSI-based electrolyte

To unveil morphological changes on the electrode surface associated with capacity fade upon aging, Figure 4 shows post-mortem electron micrographs of electrodes subjected to the voltage hold procedures of Figures 2C and 3C.

Aging at 3.95 V vs. Li/Li^+ reveals an electrode surface which resembles the pristine electrode, with no visible deposits on the electrode surface. At 4.15 V vs. Li/Li^+, the electrode surface remains mostly unchanged. The small, spherical particles observed are carbon black particles. At 4.35 V vs. Li/Li^+, the electrode surface is characterized by extensive formation of deposits. EDX analysis reveals that aluminum is detectable throughout the surface, in line with the irregular leakage current in Figure 2(D) and the current profile in Figure 1(E), both related to the dissolution of aluminum. Spot-EDX (see Figure S8) on the bright deposits confirm the enrichment in aluminum, signifying that the underlying degradation mechanism consists of current collector dissolution and subsequent

Research Article
doi.org/10.1002/batt.202300226
Chemistry Europe
European Chemical Societies Publishing

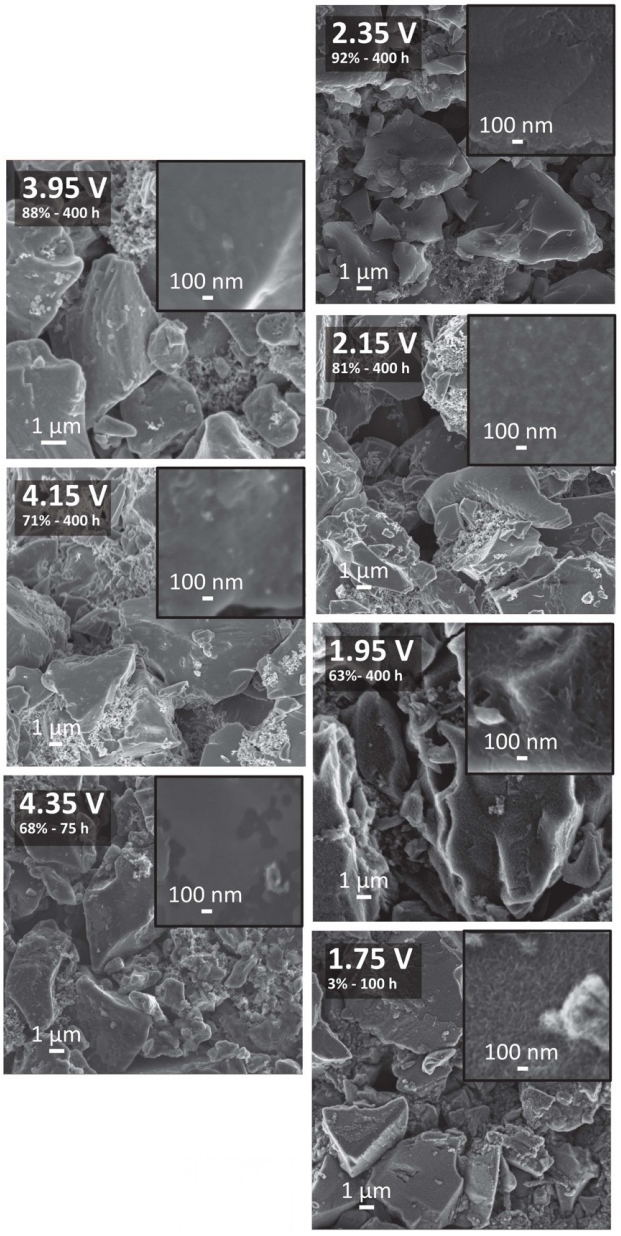

Figure 4. Post-mortem SEM of AC electrodes in 1 M LiFSI subjected to voltage hold tests for the given duration. The insets show magnified views of characteristic regions on the surface.

re-deposition of Al-rich species together with degradation products of FSI^-, likely causing extensive pore clogging.

Upon mild negative polarization to 2.35 V vs. Li/Li^+, no visible changes of the electrode surface are conceivable, consistent with the small capacity fade of 8% after 400 h. At 2.15 V vs. Li/Li^+, high magnification micrographs reveal the formation of a thin but extended film covering the surface of the AC particles. This film formation is enhanced at 1.95 V vs. Li/Li^+, exhibiting the formation of lamella-shaped surface deposits throughout the electrode. Expectedly, the film formation, which is assumed to block access of electrolyte moieties to the AC micropores, is aggravated when polarizing to 1.75 V vs. Li/Li^+, corresponding to a strong capacity fade of 97% within 100 h.

Post-mortem XPS of cycled AC electrodes in LiFSI-based electrolyte

The aging behavior of positive AC electrodes that do not exhibit marked morphological change (3.95 V and 4.15 V vs. Li/Li^+) as well as the chemical nature of the produced surface films on negatively polarized AC electrodes were further examined by XPS. Initially, the C 1s spectrum of the pristine electrode is briefly discussed (Figure 5).

The C 1s signal is composed of sp2-type carbon possessing an asymmetric peak shape due to quantum mechanic effects[9] as well as the presence of C–O, C=O, and O=C–O groups at higher chemical shift denoting oxygen-terminated groups of the AC surface. The peak at 291 eV indicates CF_2 groups from the PVDF binder[36] and the highest chemical shift corresponds to π/π^* transition around 290–291 eV in aromatic domains of the AC.[9] In Figure 6, XP spectra are presented for positive and negative electrodes satisfying the end-of-life criterion of 80% capacity retention (3.95 V and 2.15 V vs. Li/Li^+) and ones that do not (4.15 V and 1.95 V vs. Li/Li^+). To discriminate decomposition products from salt residues, an electrode dipped in LiFSI electrolyte for 24 hours without subsequent rinsing is shown as a reference.

The electrode dipped in LiFSI electrolyte shows no significant changes in the C 1s spectrum, indicating that the carbonaceous structure of AC is mostly unaffected after contact with the LiFSI electrolyte. Table 1 shows the distribution of the C 1s features of the AC electrodes after voltage held at 3.95 and 4.15 V vs. Li/Li^+. As the hold potential is increased from 3.95 V to 4.15 V vs. Li/Li^+, an intensity increase of oxygen-containing surface groups can be identified with respect to the main signal peak C_{sp2}. This indicates that the AC surface is oxidized upon aging. Oxidation of AC surface is commonly encountered with aqueous and nonaqueous electrolytes and often results in

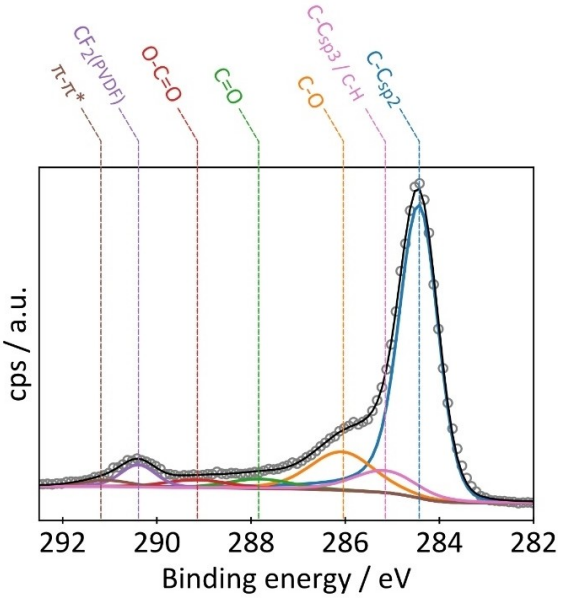

Figure 5. C 1s photoelectron spectrum of the pristine AC electrode.

Research Article
doi.org/10.1002/batt.202300226
Chemistry Europe
European Chemical Societies Publishing

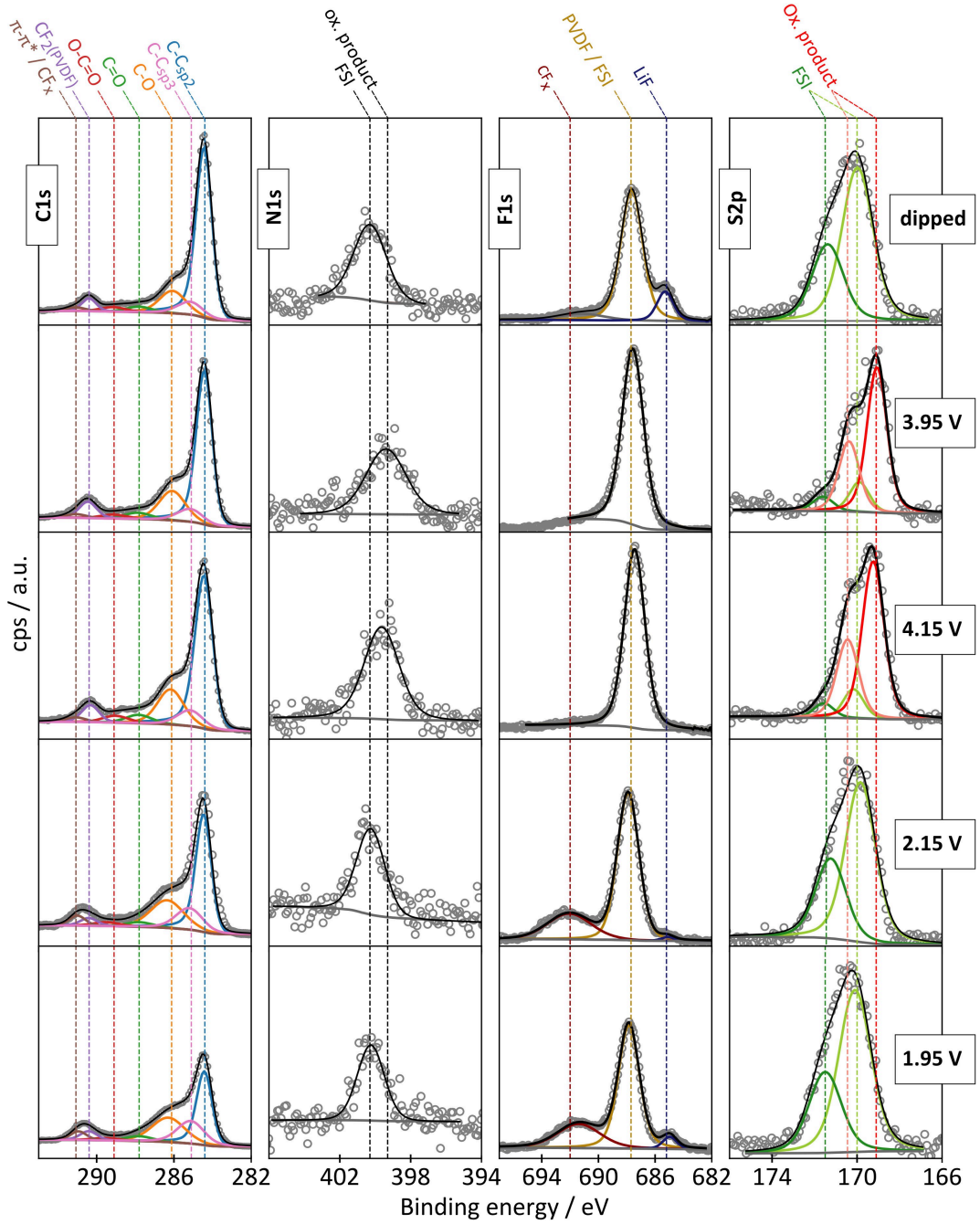

Figure 6. Deconvoluted post-mortem photoelectron spectra of AC electrodes held at the designated potentials for 400 h in LiFSI.

Table 1. Area percentages of deconvoluted C_{sp2}, C–O, C=O and O–C=O features and sum of the latter three in C 1s spectra of pristine AC electrode and positively cycled electrodes in LiFSI.

	C_{sp2}	C–O	C=O	O–C=O	$\Sigma_{C\text{-}ox}$
Pristine	64.8	14.1	3.4	2.9	19.5
3.95 V	58.22	18.47	4.00	2.59	25.06
4.15 V	55	19.4	4.56	3.82	27.82

generation of CO_2 and the occurrence of defects on the carbon surface.[8] In agreement with the findings presented in this work, a recent study involving potentiostatic aging of LIC full cells at 55 °C with an electrolyte of 1 M LiFSI in 1:1:1 mixture of EC:DEC:DMC, reported progressively increasing content of oxygenated carbon as the cell voltage is elevated from 2.2 V to 3.8 V vs. Li/Li^+. Pourhosseini et al. observed that the formation of oxygen-based surface groups upon aging of positively polarized AC electrodes coincides with a reduction of pore volume affecting pores in the range 1.2–3 nm.[37] The surface groups hinder the diffusion of ions into the deeper and smaller pores, which may explain the capacity fade at 4.15 V, as no morphological changes or deposits have been found in SEM

(Figure 4). The observed detrimental effects of oxygenated surface groups suggest that the anodic stability may substantially be improved upon surface-chemical modification of the AC material. Counterintuitively, Ding et al. observed that the complete removal of oxygen functionalities by means of hydrogenation compromises the electrochemical stability window in $LiPF_6$-based electrolytes compared to untreated AC.[9] Further studies will be dedicated towards the relation of the amount and chemical nature of AC functionalities and the long-term aging performance close to the anodic stability limit.

In negative direction, the C_{sp2} signal gradually decreases in intensity with respect to the remaining C 1s signals as the hold potential is lowered. As C_{sp2} represents the major species in activated carbon, its attenuation can be inferred to originate from coverage of the electrode surface due to electrolyte decomposition, as observed in post-mortem SEM. Formation of surface films accompanied by decrease of the C_{sp2} signal has also been detected in other studies involving electrochemical aging of activated carbon electrodes.[9]

The LiFSI-dipped electrode represents the basis for interpretation of the evolution of N 1s, F 1s and S 2p signals. The single peak at 400 eV in N 1s and the doublet peak in S 2p at 170.1 eV and 171.5 eV can be ascribed to the pristine salt on the electrode surface.[38,39] Upon anodic aging at 3.95 V vs. Li/Li^+, a new component can be observed in the S 2p region possessing a lower chemical shift, which can be attributed to an oxidation product of LiFSI (red doublet). The exact reaction mechanism remains to be identified, but the formation of bis(fluorosulfonyl)imidyl radical upon electron withdrawal is reported to be the first intermediate upon oxidative decomposition of LiFSI.[40] Together with the observed shift of N 1s by ~1 eV, we speculate that the detected oxidation product is created by homolytic bond cleavage of the S–N bond yielding a species with increased electron density located at S and N atoms. Increasing the hold potential to 4.15 V produces similar features in S 2p and N 1s regions. It is worth mentioning that the atomic percentage of S increases from 0.71% on the electrode held at 3.95 V to 1.6% for the one held 4.15 V, indicating that more of the anion oxidation product is formed on the surface in the latter case. The F 1s region does not exhibit major changes with respect to the pristine electrode, mainly depicting PVDF, demonstrating that no LiF (binding energy = 685 eV[41]) is formed during the observed decomposition of LiFSI. The LiF feature observed in the dipped electrode may be ascribed to a reaction product from spontaneous reaction of LiFSI with the surface groups of AC that remained on the electrode surface (electrode was not rinsed).

At negative polarizations of 2.15 V and 1.95 V vs. Li/Li^+, no new components have been detected in S 2p and N 1s regions. The existing signals are therefore assigned to residuals of LiFSI salt on the electrode surface. LiFSI has the tendency to undergo a reduction process resulting in F-abstraction and formation of LiF, but the reduction product would be represented by a low-shift component in the S 2p spectrum, which is not observed here.[38] The produced LiF is therefore most likely attributed to impurities or other, spontaneous chemical reactions of LiFSI on the AC surface. However, a new component at 692 eV is discernable, which is exclusively formed on negative electrodes. Formally, the signal overlaps with the binding energy of SF_6, but due to the gaseous nature of SF_6, its formation is considered unlikely. A possible explanation would be localized hyperfluorination of the carbonaceous surface as observed with graphitic ordered mesoporous carbon,[42] speculatively involving the degradation of the PVDF binder as a source for F atoms. Membreno et al. assigned the peak at 692 eV to R-CF_3 in studies of battery cathodes.[43] The enhanced $\pi - \pi^*$ signal in C 1s spectra of negative electrodes may also indicate a modification or reorganization of the carbonaceous structure.

Comparison to electrochemical stability window of $LiPF_6$

Lastly, the electrochemical performance of LiFSI is compared to $LiPF_6$ representing the most used salt in LICs. Due to the preferential uptake of (solvated) Li^+ in the pore network and expelling of (solvated) anions at negative potential, no significant impact is expected when the anion is exchanged from FSI^- to PF_6^-. Indeed, Figure 7(A–D) displays that cathodic stability in $LiPF_6$ is very similar to LiFSI. As shown in Figure 7(C), the potential of 2.1 V vs. Li/Li^+ marks the last potential with electrode capacity residing over 80% after aging for 400 h, followed by marked capacity fade of 45% as the hold potential is decreased to 1.9 V and rapid degradation at 1.7 V vs. Li/Li^+. Like LiFSI, S-values do not convey a clear picture of the safe potential window, again stressing the necessity of voltage hold tests to give a more differentiated assessment of the long-term electrochemical integrity. The cathodic limit is often neglected in reports about LICs, but the long-term experiments presented here demonstrate that reductive decomposition is not to be neglected and that a potential excursion of the AC cathode until 1.0 V vs. Li/Li^+ as reported elsewhere[44] appears to be questionable. However, in the bulk of reports on LICs, the AC potential resides well over 2.0 V vs. Li/Li^+[3,6,22,45,46] signifying that both LiFSI and $LiPF_6$ are suitable for practical use in an LIC full cell.

A marked difference between $LiPF_6$ and LiFSI is observed in the positive direction (Figure 7E–H). The highest attainable potential of $LiPF_6$ is 4.2 V vs. Li/Li^+ with over 90% capacity retention and therefore higher than in the case of LiFSI, which enabled 88% capacity retention at 3.95 V vs. Li/Li^+. This finding raises the interpretation that the FSI-solvent complex possesses a smaller oxidative stability than the PF_6-solvent complex. Changing the solvent dielectric constant and AC surface functionality may possibly enhance the oxidative stability of the FSI-solvent complex, potentially closing the gap to the state-of-the-art $LiPF_6$ electrolyte. The electrochemical performance of $LiPF_6$ at 4.4 V is heavily compromised, similar to LiFSI cycled at 4.35 V vs. Li/Li^+. However, monotonously declining leakage current at 4.4 V vs. Li/Li^+ reveals that the current collector is not involved in the degradation process, attributed to the well-known passivating behavior of $LiPF_6$ on aluminum with no significant corrosion observed up to potentials of 4.9 V vs. Li/Li^+.[29] With respect to S-values, the distinct rise for potentials higher than 4.0 V vs. Li/Li^+ is in line with the trend at long-term

Research Article
doi.org/10.1002/batt.202300226
Chemistry Europe
European Chemical Societies Publishing

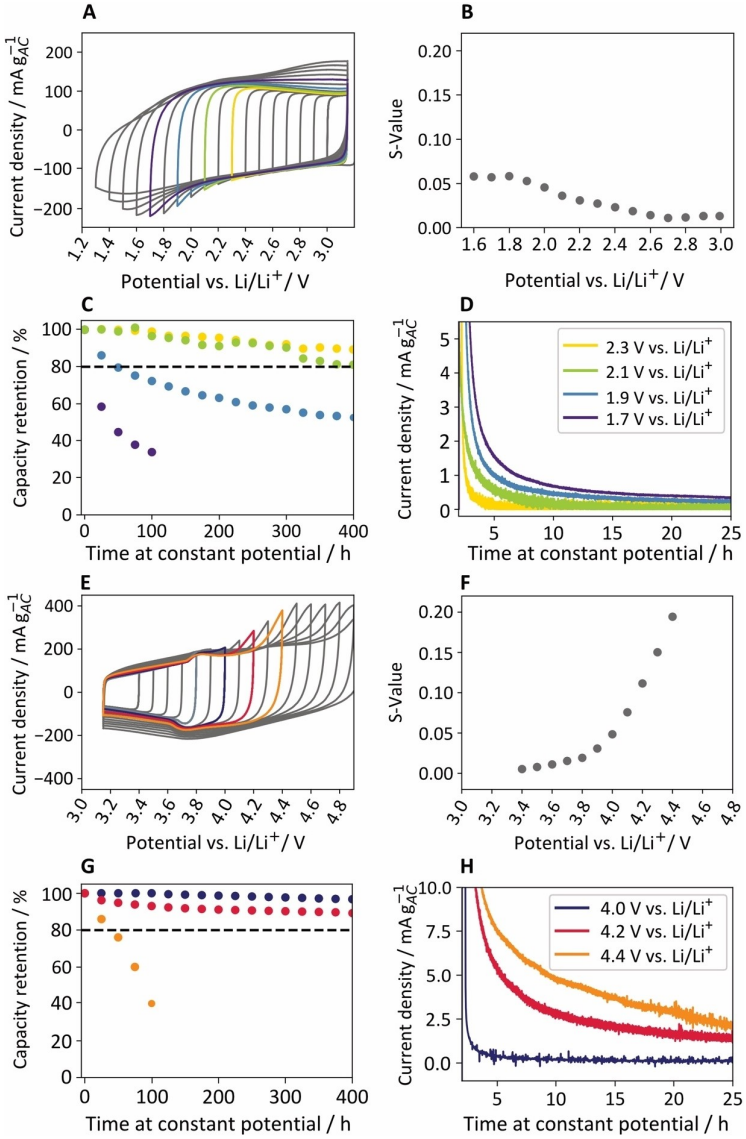

Figure 7. Cathodic and anodic stability of $LiPF_6$ on AC in three-electrode half-cell setup. A, E) Cyclic voltammograms with gradual lowering (increase) of vertex potential. B, F) S-value extracted from negative (positive) CVs. C, G) Capacity retention during voltage hold tests at selected negative (positive) potentials. D, H) Leakage currents during first 25 h of voltage hold test at negative (positive) potentials.

testing, however the high S-value (>0.1) at 4.2 V is in contradiction to the low degradation observed during voltage hold, again underlining the preliminary character of voltametric window opening experiments.

While the upper cutoff limit of 4.2 V vs. Li/Li$^+$ is in good agreement with other studies,[15,47] the cathodic potential limit is lower than in other studies investigating 1 M $LiPF_6$ + EC/DMC on AC. Wohlfahrt-Mehrens et al. identified the cathodic stability limit of YP-50 AC in 1 M $LiPF_6$ + EC/DMC (1 : 1) to be 1.5 V vs. Li/Li$^+$ by voltammetric window opening experiments.[5] However, no potential hold experiments were conducted and AC/AC symmetrical cells showed rapid capacity fade after more than 5,000 galvanostatic charge-discharge cycles, which have been attributed to early failure of the negative electrode. The wide variety of AC materials in terms of pore size distribution and the nature and amount of surface functionality complicates direct comparison to literature and highlights that control measurements must always be conducted on the same type of AC to enable sensible comparison of two given electrolytes.

Correlation of leakage current and capacity fade in $LiPF_6$ and LiFSI electrolytes

Despite being proportional to the extent of capacity fade, leakage current magnitudes are highly dependent on the electrolyte chemistry and electrode polarity. In Figure 8, the correlation between leakage current after the first 25 h at constant potential j_{25h}, electrode polarity, and capacity fade is shown. For positive polarization in LiFSI, the leakage current of 0.5 mA g_{AC}^{-1} at 3.95 V vs. Li/Li$^+$ leads to 92% capacity retention. A threefold leakage current at 4.15 V vs. Li/Li$^+$ still enables a

Research Article
doi.org/10.1002/batt.202300226
Chemistry Europe
European Chemical Societies Publishing

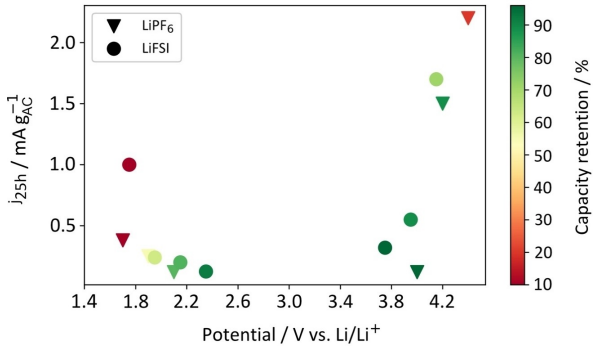

Figure 8. Specific leakage currents during first 25 h of voltage hold $j_{25\,h}$ and capacity retention after 400 h of voltage hold for AC in LiFSI and $LiPF_6$ electrolytes.

capacity retention of 72%. At negative electrode polarity, leakage currents only show a minor increase (from 0.1 to 0.2 mA g_{AC}^{-1}), however, the capacity fade progresses substantially when the hold potential is decreased from 2.35 V to 1.95 V vs. Li/Li^+. A similar discrepancy regarding anodic and cathodic leakage current and long-term degradation is observed with $LiPF_6$, where a leakage current value of 1.5 mA g_{AC}^{-1} at 4.2 V still enables capacity retention of 92%. Again, in the negative direction, a leakage current of only 0.4 mA g_{AC}^{-1} at 1.7 V vs. Li/Li^+ induces rapid electrode failure.

These findings highlight the significance of the type of chemical reactions taking place on the surface and inner pores of AC. A hypothetically large leakage current may still retain adequate device performance if the electrochemically generated species do not affect the integrity of AC, e.g., by generating gaseous products or soluble products that readily diffuse into the bulk electrolyte without further consequences for the electrode. On the other hand, a solid deposit causing extensive pore clogging (as seen in the SEM images of negative AC in Figure 4) or irreversible reactions of the surface functionality of AC is expected to induce stronger capacity fade and earlier electrode failure. Thus, we attribute the surplus of leakage current at the positive electrodes to the preferential formation of gaseous and soluble products having little direct effect on the electrode capacity. Indeed, gas formation has been observed in similar systems. In a study of propylene carbonate-based supercapacitors, the evolution of CO_2 and CO was observed at the positive electrode, with the oxygen-based surface groups arguably participating in the outgassing reactions.[48] Studies of NMC cathodes (which also possess terminal oxygen species) report the formation of vinylene carbonate from dehydrogenation of EC, the stepwise oxidation of EC to produce glycolic acid, oxalic acid and CO_2 and the oxidation of DMC to yield formic acid.[49,50] We want to highlight that all the above reaction products are either gasses or liquids soluble in carbonate media.

Implications of AC operating voltage window on LIC full cell operation

The previous aging studies in LiFSI and $LiPF_6$ were conducted in half-cell setup allowing precise control of the AC working electrode potential. It is important to highlight the significance of the voltage operation window when the AC electrode is integrated in a LIC full cell. Firstly, the meaning of voltage hold tests with respect to the operation mode of the LIC is discussed. The detected potential limits reflect the electrochemical stress on the AC electrode in a statically charged and discharged LIC (see Figure S1B, 1 and 2). The voltage hold tests in previous chapters suggest that deep discharge of the LIC should be prevented, so the AC electrode potential resides over ~2 V vs. Li/Li^+ to avoid extensive degradation due to electrolyte reduction on the AC surface. In the fully charged state, the AC electrode should not exceed the limit of 4.15 V vs. Li/Li^+ for LiFSI and 4.2 V vs. Li/Li^+ for $LiPF_6$. If the LIC is intended for continuous cycling under high C-rate, the AC electrode is exposed to the respective vertex potentials for a relatively short time. In this case, the determined stability limits in voltage hold are therefore less strict, and the AC cathode can be expected to sustain several thousand cycles even if it exceeds its ESW.

Secondly, commercial two-electrode full cells do not allow precise control and monitoring of the AC cathode. A positive potential drift of the AC cathode has been observed in LICs operated in potentiostatic[33] and under continuous cycling conditions,[3] which is caused by the continuous loss of cyclable lithium. Therefore, it is crucial to retain the Li inventory of the anode in order to limit the gradual positive potential drift of the AC cathode and the associated electrolyte degradation and/or current collector dissolution. The use of LiFSI is especially promising with respect to anode optimization, as it has been shown to yield superior SEI-forming properties than $LiPF_6$.[17] The ineffective SEI formation during prelithiation has been reported as the main cause for lithium loss in LICs operating with graphite anodes and $LiPF_6$ electrolytes.[3] The consequences of Li loss are (1) a large potential drift of the anode causing compromised cycle life and (2) a reduced total potential swing of the AC cathode, directly resulting in reduced energy density. The salt LiFSI may play a vital role in establishing a more stable SEI and therefore stabilize the potential swing of both anode and cathode during operation, resulting in enhanced cycle life. A detailed study of the potential benefits of LiFSI over $LiPF_6$ in terms of full-cell operation was however outside the scope of this work.

Lastly, the potential excursion of the AC cathode in a LIC full cell depends on other factors such as the temperature,[51] mass ratio of anode and cathode,[52] and the prelithiation degree of the anode.[3] These factors are complex and beyond the scope of this study. Nonetheless, the provided guideline dedicated to the stability window of AC in half-cell setup represents the first, crucial step towards the rational design of high-power LICs with enhanced performance and longevity.

Research Article
doi.org/10.1002/batt.202300226
Chemistry Europe
European Chemical Societies Publishing

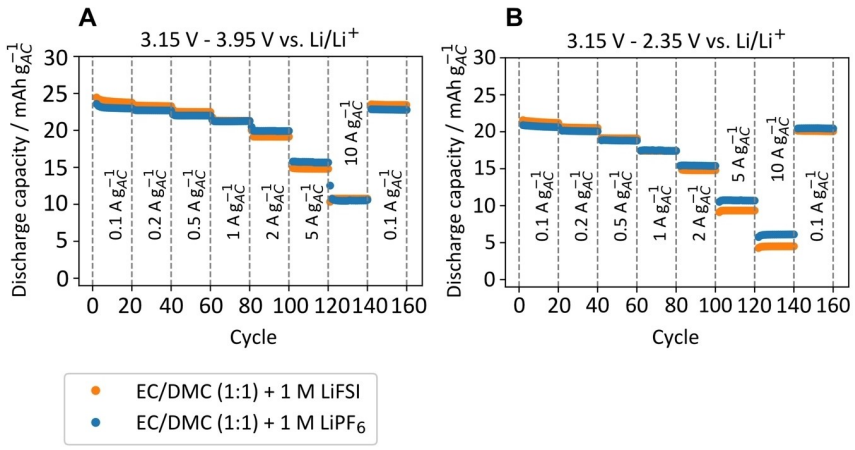

Figure 9. Discharge capacity for AC in LiFSI (orange) and $LiPF_6$ (blue) for potential excursion between A) 3.15–3.95 V vs. Li/Li^+ and B) 3.15–2.35 V vs. Li/Li^+.

Rate performance of LiFSI and $LiPF_6$ electrolytes

Complementary to the data presented thus far, which focused on the high-potential behavior of AC under low current load, the high-current capability of AC is crucial to meet the requirements of high-power LICs. Figure 9 shows rate capability tests of LiFSI and $LiPF_6$ electrolytes on AC electrodes polarized in (A) the positive direction vs. OCV and (B) the negative direction vs. OCV. The rationale for the separate investigation of positive and negative polarization is to evaluate the different contributions of cation adsorption/desorption (Li^+) and anion adsorption/desorption (FSI^- or PF_6^-) to the storage capacity. The potential excursion is limited to ± 0.8 V to stay within the non-faradaic domain and avoid irreversible side reactions.

The results indicate that the storage capacity and rate performance is not significantly influenced by the exchange of PF_6^- by FSI^-. However, both for LiFSI and $LiPF_6$, there is a pronounced discrepancy between the rate performance in anodic and cathodic directions, with the first being always superior to the latter at any given current. Considering the ion diameter of Li^+ being significantly smaller than the molecular diameter of the anions (see Table 2), this finding is unexpected as smaller ion dimensions would be associated with an increased ion population on the AC surface and higher storage capacity. However, the high charge-density Li^+ ion is reported to engage in strong solvation with EC, preferentially forming $[Li(EC)_n]^+$ ($n = 3$–4), which are also formed in EC/DMC solvents which have a substantially smaller dielectric constant.[53–55] In contrast, the PF_6^- anion is reported to have much weaker interaction with EC, with Li^+ participating in the first solvation sheath and PF_6^- located in the second solvation sheath as evidenced by crystallographic studies.[54] A similar argumentation holds for FSI^-, which is attested to have weak solvation by cyclic carbonates due to its large self-diffusion coefficient.[56] The formation of rather bulky $[Li(EC)_n]^+$ with approximated diameter of 17.8 Å[53] and low propensity of unsolvated Li^+ suggests that some of the smallest pores of the AC material are inaccessible for ion adsorption. In contrast, weaker solvation of anions and facilitated (partial) desolvation upon entering the smallest pores enables higher storage capacity when AC is positively polarized.

Table 2. Diameters of ionic and molecular species. Values for FSI^- and PF_6^- ions were derived from jsmol simulation.

Species	Diameter [Å]
Li^+	0.76[57]
$[Li(EC)_4]^+$	~17[53]
FSI^-	5.4
PF_6^-	3.15

Conclusions

In this work, the performance and stability of a commercial AC in the electrolyte 1 M LiFSI in EC/DMC (1:1) is investigated, with the aim of assessing the feasibility of this salt for use in LICs. Based on voltage hold measurements, good long-term stability is achieved with an upper cut-off voltage of 3.95 V vs. Li/Li^+, potentially enabling cell voltages of ~3.8 V when combined with graphite or silicon-based anodes (operating at ~0.1 V vs. Li/Li^+) in LIC full cells. The lower cut-off voltage was determined to be 2.15 V vs. Li/Li^+.

The systematic comparison of CV, leakage current analysis and capacity retention upon voltage hold highlighted the importance of the latter method to provide a realistic assessment of the ESW of LiFSI on a commercial AC. Thus, voltage hold tests are recommended to account for slow-current processes that tend to be overlooked in CV and leakage current analysis. Similarly, the information provided by CV of current collector foils must be complemented by long-term protocols such as CA to assess the potential-dependent durability of passivation layers. A stability limit of 4.15 V vs. Li/Li^+ was identified for carbon-primed aluminum current collectors, with the carbon coating successfully mitigating the occurrence of corrosion pits.

The morphological and surface-chemical post-mortem analysis of AC electrodes in LiFSI revealed the oxidation of the FSI^- anion, as evidenced by the presence of new S 2p and N 1s photoemission features and increasing number of oxygenated species on the AC as the main processes causing capacity fade at positive polarization. These aging phenomena occurred at potentials $\leq$ 4.15 V, i.e., the anodic stability of AC exposed to LiFSI is limited by electrolyte decomposition, and not the corrosion of the aluminum current collector.

Upon negative polarization, SEI-like film deposition, potentially causing pore-clogging of the microporous AC, is responsible for capacity loss. Around the lower cut-off, relatively low leakage currents were associated with poor capacity retention, while significantly higher leakage currents were observed around the highest cut-off voltage, indicating less detrimental side reactions at the high anodic potentials. Comparison of LiFSI to state-of-the-art salt $LiPF_6$ revealed on-par rate capability, but a reduced anodic stability window of the LiFSI electrolyte. Future efforts should be dedicated towards the stabilization of (solvated) FSI^- anion against oxidative decomposition through the following approaches. On the one hand, the solvation environment of LiFSI can be altered by changing the solvent dielectric constant through different ratios of EC:DMC, or other solvent mixtures. On the other hand, the pore size distribution of the AC host material can be modified to change the local chemical environment of pore-confined LiFSI. Finally, the accelerated electrolyte decomposition by oxygen-based surface groups needs to be addressed. Reducing the amount of oxygen-based reactive surface groups, e.g., by reductive treatment, will be pursued in upcoming studies to mitigate parasitic reactions and increase the upper cut-off potential.

Experimental

Materials

YEC-8 activated carbon was purchased from Fuzhou Yihuan Carbon Co. Ltd. Super P® conductive carbon black (CB, $\geq$ 99%), was purchased from VWR. PTFE suspension (20 vol.%), DMC, EC and $LiPF_6$ were supplied by Sigma-Aldrich in battery grade levels and used without further purification. N-methylpyrrolidone (NMP) was purchased from Sigma-Aldrich. Polyvinylidene difluoride (PVDF) was obtained from Arkema. LiFSI (99.9%, $H_2O < 20$ ppm, $Cl^- \leq$ 100 ppm) was supplied by Solvionic and dried for 48 h at 100 °C under vacuum. Carbon-primed aluminum foil (c-Al) was purchased from MTI Corp. and heated at 120 °C under vacuum prior to electrode casting. Molecular sieves of 3 Å were purchased from Sigma-Aldrich. Whatman GF-A separators with thickness 260 µm were dried at 10^{-2} mbar for 48 h. Solupor®7P03A Polymer separators were purchased from Lydall Performance Materials and dried at 65 °C overnight. Ferrocene (98%) was purchased from Sigma-Aldrich and used without further purification. The polycrystalline platinum electrode used for electrode calibration experiments was purchased from Pine Research Instrumentation, Inc.

Electrolyte preparation

The mixing of electrolytes was performed in a glove box with oxygen and water levels < 0.1 ppm. Prior to salt addition, a binary mixture of EC and DMC (weight ratio 1:1) was stored over molecular sieves 3 Å for 48 h to remove trace water. The salts were then added at room temperature to obtain the electrolytes 1 M LiFSI in EC/DMC (1:1) and 1 M $LiPF_6$ in EC/DMC (1:1), further denoted as LiFSI and $LiPF_6$, respectively. The water content of the prepared electrolytes varied between 15 ppm and 22 ppm as measured by coulometric Karl-Fischer Titration using Mettler Toledo C10s KF Titrator.

Electrode preparation

Activated carbon working electrodes (AC-WE) were prepared by adding AC, CB, and PVDF in weight ratio 90:5:5 to NMP (liquid: solid weight ratio = 3:1) and stirring at 1000 rpm overnight at room temperature. The slurry was tape-cast on c-Al foil (150 µm wet casting thickness) and dried overnight at 80 °C. Free-standing oversized activated carbon counter electrodes (AC-CE) and activated carbon quasi-reference electrodes (AC-QRE) were prepared by mixing AC, PTFE, and CB in deionized water in weight ratio 85:10:5 and stirring overnight at 400 rpm under evaporation at 80 °C. The resulting mass was kneaded and rolled out using a calendering machine from which electrodes were cut. For electrode dimensions and active material loadings *m*, please refer to Table 3. AC-WEs, AC-QREs and AC-CEs were dried at 120 °C at 10^{-2} mbar for 48 h before transferring them into an argon-filled glove box with oxygen and water levels < 0.1 ppm.

Cell assembly and electrochemical testing

The ESW of AC electrodes was evaluated via cyclic voltammetry (CV) and voltage hold tests in three-electrode Swagelok-type cells with polyetheretherketone (PEEK)-protected steel plungers equipped with AC-WE, AC-CE and AC-QRE. For characterization of $LiPF_6$ electrolyte, a lithium disk was used as a reference electrode due to non-negligible potential drift of AC-QRE in this electrolyte[58] (for interconversion between AC-QRE and Li/Li^+ reference potentials in LiFSI, see Figure S2 in the Supporting Information). Whatman GF-A separators were soaked with 200 µL of electrolyte and

Table 3. Overview of cell setups for electrochemical measurements.

Material	Experiments	Cell	WE	CE	RE
AC	Cyclic voltammetry Voltage hold	Swagelok	AC (ø = 12 mm, $h = 75 \pm 20$ µm, $m = 3.00$–3.65 $mg_{AC}cm^{-2}$)	AC (ø = 12 mm, $h = 0.8$ mm, m ~50 $mg_{AC}cm^{-2}$)	AC or Li (ø = 6 mm)
AC	Rate capability	PAT-cell	AC (ø = 18 mm, $h = 75 \pm 20$ µm, $m = 3.00$ $mg_{AC}cm^{-2}$)	AC (ø = 18 mm, $h = 0.3$ mm, m ~15 $mg_{AC}cm^{-2}$)	Li-ring
Current collector	Cyclic voltammetry Chronoamperometry	Pouch cell	Al/c-Al (ø = 12 mm)	Li (ø = 12 mm)	n.a.

the cells were rested for four days to ensure sufficient wetting and negligible potential drift of the reference electrode. To facilitate post-mortem analysis, a Solupor 7P03A separator was placed between the AC-WE and glass fiber separator. CV on AC-WEs (scan rate 1 $mV\,s^{-1}$) was performed after a method described by Weingarth et al.[34] The upper vertex potential was increased or decreased from OCV of ~3.15 V vs. Li/Li^+ by 100 mV in either positive or negative direction for subsequent scans and an S-value was determined as $S = 1 - \frac{Q_{forward}}{Q_{backward}}$ with $Q_{forward}$ and $Q_{backward}$ denoting the integrated charge during forward and backward sweep, respectively. Voltage hold tests were performed according to Ruschhaupt et al.[26] and the procedure is illustrated in Figure S3. The AC-WE was held at a constant potential for 25 h with intermittent galvanostatic charge discharge at 0.1 $A\,g_{AC}^{-1}$ for capacity determination. The total time spent at constant potential was 400 h, or less in case of premature electrode degradation. Several cells were assembled for each electrolyte and magnitude of polarity to account for reproducibility and to reduce statistical spread of cell performances, while a representative cell was selected for postmortem analysis.

Rate capability experiments were conducted using 3-electrode PAT cells to avoid the influence of varying cell stack pressure on iR drop. PAT cells were equipped with AC-WE, oversized AC-CE, Li-ring reference electrode and Whatman GF-A separator soaked with 200 μL of electrolyte. To reduce cell resistance, the loading of AC-CE was decreased (see Table 3). Specific currents ranged from 0.1 to 10 $A\,g_{AC}^{-1}$.

For the study of aluminum current collectors, two-electrode pouch cells were assembled by sandwiching the respective foil and lithium disk serving as counter and reference electrode between Solupor 3P07 separators soaked with 40 μL of electrolyte. CV experiments were performed with a sweep rate of 0.1 $mV\,s^{-1}$. Chronoamperometry (CA) experiments were carried out with a charging current of 50 μA to the set potential, and a potential hold step of 24 hours. Table 3 gives an overview of the used cell setups and electrode parameters.

All electrochemical measurements were performed using a Biologic VMP-300 potentiostat except for voltage hold tests on AC-WEs, which were conducted on a Biologic BCS-805 battery cycler.

Material analysis and post-mortem characterization

Prior to post-mortem analysis, the electrodes were retrieved from the cells and rinsed in DMC. Scanning electron microscopy (SEM) was conducted using ThermoFisher Scientific Apreo SEM with T2 detector, accelerating voltages of 5 kV and beam current of 0.10 nA. Energy-dispersive X-ray analysis (EDX) was performed on the same instrument with an accelerating voltage of 20 kV. X-ray photoelectron spectroscopy (XPS) was carried out on Kratos Analytical Axis Ultra DLD using monochromatic Al K-α as the radiation source, operating at 10 kV and 10 mA emission current. Multiple scans were acquired for high-resolution elemental regions at a pass energy of 20 eV and averaged to enhance signal-to-noise-ratio. Nitrogen sorption analysis was performed on Micromeritics 3Flex BET analyzer using N_2 as adsorbate. NLDFT pore size distribution was obtained from the BET isotherms assuming Tarazona cylindrical pore model.

Data processing

Electrochemical data from voltage hold tests was processed using a custom script in Python 3. Data analysis and peak deconvolution of X-ray photoelectron spectra was carried out in CasaXPS. Molecular dimensions for FSI^- and PF_6^- anions were derived from Jsmol simulation software after geometrical optimization. The distance of the farthest atoms within the molecule was taken as the molecule diameter.

Author Contributions

Philipp Schweigart: Conceptualization, investigation, data acquisition & curation, writing – original draft, writing – review & editing.

Prof. Ann Mari Svensson: Conceptualization, investigation, funding acquisition, writing – original draft, writing – review & editing.

Dr. Samson Yuxiu Lai: Conceptualization, investigation, writing – original draft, writing - review & editing.

Obinna Egwu Eleri: Investigation, validation, writing – review & editing.

Dr. Inger-Emma Nylund: Investigation, assistance with SEM imaging, writing – review & editing.

Acknowledgements

The authors gratefully acknowledge financial support of this work by the Research Council of Norway (contract number 306400) within the project "Norwegian Giga Battery Factories (NorGiBatF)". The responsibility for the content of this publication is up to the authors.

Conflict of Interests

The authors declare no conflict of interest.

Keywords: activated carbon · aging · electrochemical stability window · LiFSI · lithium-ion capacitor

[1] L. Jin, C. Shen, A. Shellikeri, Q. Wu, J. Zheng, P. Andrei, J. G. Zhang, J. P. Zheng, *Energy Environ. Sci.* **2020**, *13*, 2341.
[2] L. Jin, J. Yuan, A. Shellikeri, R. Naderi, N. Qin, Y. Lu, R. Fan, Q. Wu, J. Zheng, C. Zhang, J. P. Zheng, *Batteries & Supercaps* **2021**, *4*, 749.
[3] S. R. Sivakkumar, A. G. Pandolfo, *Electrochim. Acta* **2012**, *65*, 280.
[4] S. S. Zhang, *Batteries & Supercaps* **2020**, *3*, 1137.
[5] T. Zhang, B. Fuchs, M. Secchiaroli, M. Wohlfahrt-Mehrens, S. Dsoke, *Electrochim. Acta* **2016**, *218*, 163.
[6] M. Arnaiz, V. Nair, S. Mitra, J. Ajuria, *Electrochim. Acta* **2019**, *304*, 437.
[7] K. Xu, *Chem. Rev.* **2014**, *114*, 11503.
[8] K. Naoi, *Fuel Cells* **2010**, *10*, 825.
[9] Z. Ding, V. Trouillet, S. Dsoke, *J. Electrochem. Soc.* **2019**, *166*, A1004.
[10] N. Batisse, E. Raymundo-Piñero, *ACS Appl. Mater. Interfaces* **2017**, *9*, 41224.
[11] T. Aida, I. Murayama, K. Yamada, M. Morita, *J. Electrochem. Soc.* **2007**, *154*, A798.
[12] P. Azaïs, L. Duclaux, P. Florian, D. Massiot, M. A. Lillo-Rodenas, A. Linares-Solano, J. P. Peres, C. Jehoulet, F. Béguin, *J. Power Sources* **2007**, *171*, 1046.
[13] Y. Liu, B. Soucaze-Guillous, P. L. Taberna, P. Simon, *J. Power Sources* **2017**, *366*, 123.
[14] M. Tokita, N. Yoshimoto, K. Fujii, M. Morita, *Electrochim. Acta* **2016**, *209*, 210.
[15] O. E. Eleri, J. Pires, F. T. Huld, S. Lu, P. Schweigart, A. M. Svensson, F. Lou, Z. Yu, *Sustain. Energy Fuels* **2023**, *7*, 1846.

[16] D. Stępień, Z. Zhao, S. Dsoke, *J. Electrochem. Soc.* **2018**, *165*, A2807.
[17] S. J. Kang, K. Park, S. H. Park, H. Lee, *Electrochim. Acta* **2018**, *259*, 949.
[18] K. Asheim, P. E. Vullum, N. P. Wagner, H. F. Andersen, J. P. Mæhlen, A. M. Svensson, *RSC Adv.* **2022**, *12*, 12517.
[19] H. B. Han, S. S. Zhou, D. J. Zhang, S. W. Feng, L. F. Li, K. Liu, W. F. Feng, J. Nie, H. Li, X. J. Huang, M. Armand, Z. Bin Zhou, *J. Power Sources* **2011**, *196*, 3623.
[20] Y. Cai, H. Zhang, Y. Cao, Q. Wang, B. Cao, Z. Zhou, F. Lv, W. Song, D. Duo, L. Yu, *J. Power Sources* **2022**, *535*, 231481.
[21] J. Liu, Y. Cai, H. Pang, B. Cao, C. Luo, Z. Hu, C. Xiao, H. Zhang, F. Lv, Y. Cao, L. Yu, *Chin. Chem. Lett.* **2022**, *33*, 4061.
[22] X. Sun, X. Zhang, K. Wang, Y. An, X. Zhang, C. Li, Y. Ma, *Electrochim. Acta* **2022**, *428*, 1.
[23] P. Jezowski, O. Crosnier, E. Deunf, P. Poizot, F. Béguin, T. Brousse, *Nat. Mater.* **2018**, *17*, 167.
[24] A. Gabryelczyk, S. Ivanov, A. Bund, G. Lota, *J. Energy Storage* **2021**, *43*, 103226.
[25] X. Wu, Z. Du, *Electrochem. Commun.* **2021**, *129*, 107088.
[26] P. Ruschhaupt, S. Pohlmann, A. Varzi, S. Passerini, *Batteries & Supercaps* **2020**, *3*, 698.
[27] C. Li, S. Zeng, P. Wang, Z. Li, L. Yang, D. Zhao, J. Wang, H. Liu, S. Li, *Trans. Nonferrous Met. Soc. China* **2021**, *31*, 1439.
[28] M. Onsrud, A. O. Tezel, S. Fotedar, A. M. Svensson, *SN Appl. Sci.* **2022**, *4*, 225.
[29] E. Yoon, J. Lee, S. Byun, D. Kim, T. Yoon, *Adv. Funct. Mater.* **2022**, *32*, 2200026.
[30] H. Yang, K. Kwon, T. M. Devine, J. W. Evans, *J. Electrochem. Soc.* **2000**, *147*, 4399.
[31] S. Theivaprakasam, G. Girard, P. Howlett, M. Forsyth, S. Mitra, D. MacFarlane, *npj Mater. Degrad.* **2018**, *2*, 13.
[32] R. S. Kühnel, A. Balducci, *J. Power Sources* **2014**, *249*, 163.
[33] T. Saito, K. Kuwahara, S. Ishikawa, S. Shiraishi, *Electrochemistry* **2020**, *88*, 57.
[34] D. Weingarth, H. Noh, A. Foelske-Schmitz, A. Wokaun, R. Kötz, *Electrochim. Acta* **2013**, *103*, 119.
[35] M. C. G. Santos, G. G. Silva, R. Santamariá, P. F. R. Ortega, R. L. Lavall, *J. Phys. Chem. C* **2019**, *123*, 8541.
[36] M. D. Duca, C. L. Plosceanu, T. Pop, *J. Appl. Polym. Sci.* **1998**, *67*, 2125.
[37] S. E. M. Pourhosseini, A. Bothe, A. Balducci, F. Beguin, P. Ratajczak, *Energy Storage Mater.* **2021**, *38*, 17.
[38] B. Philippe, R. Dedryvèire, M. Gorgoi, H. Rensmo, D. Gonbeau, K. Edström, *J. Am. Chem. Soc.* **2013**, *135*, 9829.
[39] A. Kotronia, H. D. Asfaw, C. W. Tai, M. Hahlin, D. Brandell, K. Edström, *ACS Appl. Mater. Interfaces* **2021**, *13*, 3867.
[40] I. A. Shkrob, T. W. Marin, Y. Zhu, D. P. Abraham, *J. Phys. Chem. C* **2014**, *118*, 19661.
[41] V. Sharova, A. Moretti, T. Diemant, A. Varzi, R. J. Behm, S. Passerini, *J. Power Sources* **2018**, *375*, 43.
[42] P. F. Fulvio, G. M. Veith, J. L. Adcock, S. S. Brown, R. T. Mayes, X. Wang, S. M. Mahurin, B. Guo, X. G. Sun, A. A. Puretzky, C. M. Rouleau, D. B. Geohegan, S. Dai, *J. Mater. Chem. A* **2013**, *1*, 9414.
[43] N. Membreño, K. Park, J. B. Goodenough, K. J. Stevenson, *Chem. Mater.* **2015**, *27*, 3332.
[44] V. Khomenko, E. Raymundo-Piñero, F. Béguin, *J. Power Sources* **2008**, *177*, 643.
[45] X. Sun, X. Zhang, H. Zhang, N. Xu, K. Wang, Y. Ma, *J. Power Sources* **2014**, *270*, 318.
[46] M. Saito, K. Takahashi, K. Ueno, S. Seki, *J. Electrochem. Soc.* **2016**, *163*, A3140.
[47] X. Sun, Y. An, X. Zhang, K. Wang, C. Yuan, X. Zhang, C. Li, Y. Xu, Y. Ma, *Batteries* **2022**, *9*, 11.
[48] K. Naoi, S. Ishimoto, J. I. Miyamoto, W. Naoi, *Energy Environ. Sci.* **2012**, *5*, 9363.
[49] B. L. D. Rinkel, D. S. Hall, I. Temprano, C. P. Grey, *J. Am. Chem. Soc.* **2020**, *142*, 15058.
[50] H. Luo, B. Zhang, H. Zhang, Q. Zheng, X. Wu, Y. Yan, Z. Li, Y. Tang, W. Hao, G. Liu, Y. Hong, J. Ye, Y. Qiao, S.-G. Sun, *J. Phys. Chem. Lett.* **2023**, *14*, 4565.
[51] D. Karimi, H. Behi, J. Van Mierlo, M. Berecibar, *Molecules* **2022**, *27*, 3119.
[52] X. Guo, R. Gong, N. Qin, L. Jin, J. Zheng, Q. Wu, J. P. Zheng, *J. Electroanal. Chem.* **2019**, *845*, 84.
[53] W. Cui, Y. Lansac, H. Lee, S. T. Hong, Y. H. Jang, *Phys. Chem. Chem. Phys.* **2016**, *18*, 23607.
[54] P. Y. Zavalij, S. Yang, M. S. Whittingham, *Acta Crystallogr. Sect. B* **2004**, *60*, 716.
[55] C. L. Berhaut, D. Lemordant, P. Porion, L. Timperman, G. Schmidt, M. Anouti, *RSC Adv.* **2019**, *9*, 4599.
[56] J. Neuhaus, D. Bellaire, M. Kohns, E. von Harbou, H. Hasse, *Chem. Ing. Tech.* **2019**, *91*, 1633.
[57] N. Q. Khuyen, Z. Zondaka, M. Harjo, J. Torop, T. Tamm, R. Kiefer, *Polymers (Basel).* **2019**, *11*, 849.
[58] P. W. Ruch, D. Cericola, M. Hahn, R. Kötz, A. Wokaun, *J. Electroanal. Chem.* **2009**, *636*, 128.

Manuscript received: May 30, 2023
Revised manuscript received: July 25, 2023
Accepted manuscript online: July 26, 2023
Version of record online: August 8, 2023